

# A faint red stellar halo around an edge-on disc galaxy in the Hubble Ultra Deep Field

Stefano Zibetti<sup>1\*</sup> and Annette M. N. Ferguson<sup>1</sup>

<sup>1</sup>Max-Planck-Institut für Astrophysik, Karl-Schwarzschild-Str. 1, D-85748 Garching bei München, Germany

Accepted . Received ; in original form 2004 April 23

## ABSTRACT

We analyse the detailed structure of a highly-inclined ( $i \gtrsim 80^\circ$ ) disc galaxy which lies within the Hubble Ultra Deep Field (UDF). The unprecedented depth of the UDF data allow disc and extraplanar emission to be reliably traced to surface brightness levels of  $\mu_{V,i,z} \sim 29 - 30$  mag arcsec<sup>-2</sup> (corresponding to rest-frame equivalents of  $\mu_{g,r,i} \sim 28 - 29$  mag arcsec<sup>-2</sup>) in this redshift  $z = 0.32$  system. We detect excess emission above the disc which is characterised by a moderately-flattened ( $b/a \sim 0.6$ ) power-law ( $I \propto R^{-2.6}$ ). The structure and colour of this component are very similar to the stellar halo detected in an SDSS stacking analysis of local disc galaxies (Zibetti, White, & Brinkmann 2004) and lend support to the idea that we have detected a stellar halo in this distant system. Although the peculiar colours of the halo are difficult to understand in terms of normal stellar populations, the consistency found between the UDF and SDSS analyses suggests that they cannot be easily discounted.

**Key words:** galaxies: haloes, galaxies: structure, galaxies: photometry, galaxies: spiral

## 1 INTRODUCTION

In the currently-favoured  $\Lambda$ CDM framework, galaxy formation proceeds hierarchically with small structures forming first and later merging and accreting to form large galaxies. In these models, a significant fraction the stars which reside in the stellar halo and thick disc are tidally-stripped from small satellites as they fall within the host potential (e.g. Abadi, Navarro, Steinmetz & Eke 2003). The structure, composition and ubiquity of these faint stellar components are thus expected to reflect the details of the galaxy assembly process (e.g. Bullock & Johnston 2004).

Observations of stellar haloes and thick discs in external galaxies are extremely challenging. These faint components typically have surface brightnesses  $\mu_R \gtrsim 28$  mag arcsec<sup>-2</sup>, which corresponds to  $\gtrsim 7$  magnitudes fainter than the sky. Measurements of diffuse emission require flat-fielding and sky subtraction uncertainties, as well as scattered light effects, to be significantly less than 0.1 per cent. Until recently, few observational constraints were available with which to confront models. While there have been some detections of faint stellar components in external galaxies (e.g. Sackett et al. 1994; Morrison et al. 1997; Lequeux et al. 1998; Abe et al. 1999), there have also been non-detections (e.g. Zheng et al. 1999; Fry et al. 1999), leading one to question to what extent the results re-

flect real variance as opposed to systematic effects (see Zibetti, White, & Brinkmann 2004, hereafter Z04, for a full discussion). The alternative technique of using wide-area resolved star counts to study stellar haloes sidesteps the difficulties inherent in quantifying extremely faint diffuse emission, but can only be applied to a handful of nearby galaxies (e.g. Ferguson et al. 2002).

Recently Z04 have conducted the first statistical study of stellar halo emission by stacking  $\gtrsim 1000$  homogeneously rescaled edge-on galaxies from the Sloan Digital Sky Survey (SDSS). This technique has allowed quantitative analysis of the “mean” stellar halo to  $\mu_r \sim 31$  mag arcsec<sup>-2</sup>. These authors find a halo characterised by a moderately-flattened ( $b/a \sim 0.6$ ) power-law ( $I \propto R^{-2}$ ) and puzzling colours ( $g - r = 0.65$ ,  $r - i = 0.6$ ) that cannot be easily explained by normal stellar populations. The detection of flatter red stellar envelopes around extreme late-type edge-on disc galaxies by Dalcanton & Bernstein (2002) may represent the higher surface brightness regions of these haloes.

The recent release of the Hubble Ultra Deep Field (UDF), a public survey carried out with the Advanced Camera for Surveys using Director’s Discretionary time in Cycle 12 (Beckwith, Somerville & Stiavelli 2003), provides a rare opportunity to quantitatively study galaxy structure to the depths where halo emission should prevail. This *Letter* reports the detection of a faint red stellar halo around a  $z = 0.32$  edge-on galaxy in the UDF.

\* E-mail: zibetti@MPA-Garching.MPG.DE

## 2 OBSERVATIONS AND ANALYSIS

The Hubble Ultra Deep Field (UDF) consists of 400 orbits of integration on a single  $11.3 \text{ arcmin}^2$  field lying within the Chandra Deep Field South GOODS area, centred at RA=  $03^{\text{h}}32^{\text{m}}39^{\text{s}}.0$ , Dec=  $-27^{\circ}47'29''.1$  (J2000). Four filters have been utilised: *B*(F435W), *V*(F606W) (each for 56 orbits, 37.5 hours) and *i*(F775W), *z*(F850LP) (each for 144 orbits, 96.4 hours). The UDF represents the deepest observations yet obtained with HST, or any ground-based telescope.

We focus on a relatively large, well-formed disc galaxy located at RA=  $03^{\text{h}}32^{\text{m}}41^{\text{s}}.1$ , Dec=  $-27^{\circ}48'52''.9$  (J2000). This galaxy is clearly detected in all 4 bands and is identified with source #31611 at  $z = 0.322$  in the COMBO-17 photometric redshift survey of Wolf et al. (2004). The high inclination of this system makes it an ideal target for a study of faint extraplanar emission. At this redshift, 1 arcsec=4.7 kpc and the lookback time is 3.6 Gyr<sup>1</sup>. We note the presence of a ring-like structure of blue knots lying along the western major axis (see Fig. 1(a)); this structure has a photometric redshift of unity according to Wolf et al. (2004) and thus appears as a chance alignment.

Our analysis is based on the reduced UDF data v1.0 released to the community by STScI on March 9, 2004<sup>2</sup>. The data were pre-processed using the standard ACS/WFC pipeline and subsequently combined using the Multidrizzle package. The observations were obtained using a 4-point dither pattern to provide sub-pixel sampling, as well as a larger-scale pattern to cover the 2 arcsec gap between the ACS/WFC chips. The final pixel scale after drizzling is 0.6 of the original, corresponding to 0.03 arcsec. Note that all magnitudes are on the *AB*-system with zero-points provided by STScI. We have additionally applied a correction for Galactic extinction using Schlegel et al. (1998).

Using the geometric parameters obtained from *STSDAS-ellipse* fitting of the *i*-band isophotes, we have extracted  $1200 \times 1200 \text{ pixel}^2$  frames in each band, centred on the galaxy and rotated according to the average position angle of the isophotes at  $\mu_i \sim 24 \text{ mag arcsec}^{-2}$ . The RGB colour composite image of the galaxy is shown Fig. 1 (a), where we use the *B*-band image for the blue channel, *V* for the green, and *i* + *z* for the red.

We use SExtractor v2.3 (Bertin & Arnouts 1996) to extract very low signal-to-noise segmentation images of the frames, adopting a  $5 \times 5 \text{ pix}^2$  gaussian smoothing kernel ( $\sigma = 2 \text{ pixels}$ ), a 1- $\sigma$  detection threshold and a 25 pixel minimum detection area. After excluding the segment(s) corresponding to the galaxy and manually editing the mask to include sources that were not correctly deblended from the galaxy, we combine the masks in the four bands and “grow” the resulting mask by 2 pixels, in order to have better coverage of the extended diffuse sources. The masked *i* + *z*-band image is shown in Fig. 1 (b), with an enhanced contrast in order to show the lowest intensity levels.

Visual inspection indicates that the galaxy is close to edge-on and this is confirmed by the measured isophotal axial ratio of 0.2 at  $\mu_i \sim 24 \text{ mag arcsec}^{-2}$ . Assuming the standard formula for an infinitely thin disc ( $\cos i = b/a$ ), this

corresponds to an inclination of  $78^\circ$ . For the more realistic case of finite thickness, the inclination will be somewhat greater than this. Fig. 1 a) also suggests a late-type classification for the galaxy based on prominent star-forming spiral arms, a significant amount of dust in the inter-arm region and a very small bulge, if present at all. In Fig. 1 b), one can clearly see the presence of red extraplanar emission which will be analysed in significant detail in the following section.

Although the UDF science images are already background subtracted, we estimate and subtract the residual average local background using an annulus (inner radius= 400 pixels or 56 kpc, width = 200 pixels or 28 kpc) around the galaxy on the masked images. This annulus is chosen to lie outside the region where we might reasonably expect faint halo emission to be present. The maximum correction corresponds to a surface brightness of  $\sim 31 \text{ mag arcsec}^{-2}$  (measured in the *z*-band); comparison to the faintest measured *z*-band surface brightness indicates that the level of uncertainty due to the background is no more than 20%. Smaller background uncertainties are found in all other bands.

The primary photometric analysis is performed on the masked images using an in-house developed C code which provides us with the average pixel value as a function of radius within a wedge-shaped region with apex located at the galaxy centre. As we believe the galaxy is close to edge-on, this technique provides an alternative to making simple major and minor axis cuts and is particularly well-suited to the study of very faint emission at large radius since relatively more pixels are averaged in these parts. Errors are attached by taking into account both the count statistics and the typical rms background fluctuations occurring on the same scale as the aperture. The latter quantity is computed by evaluating the surface brightness in a number of non-overlapping apertures spread throughout the frame and located at least 400 pixels from the centre of the galaxy.

## 3 RESULTS

In Fig. 2 and 3, we show the surface brightness profiles measured along the major and minor axes of the galaxy respectively. As described in the legend, the different coloured symbols correspond to the four bands. The asymmetry seen in the inner regions of both profiles attests to the presence of spiral structure and dust lanes in these parts. We include these regions for completeness, but note their interpretation is complicated; our main focus is the behaviour of the profiles at very large radius.

The major axis profile is extracted using wedges aligned with the  $+x$  and  $-x$ -axes and with a small opening angle of  $10^\circ$  (see Fig. 2). While a warp is present in the outer parts of the disk, our extraction method involves summing over many pixels at large radius and is thus not significantly affected by the deviation from the midplane. In all four bands, the profile shows a profound change in slope at  $\sim 3 \text{ arcsec}$ . By fitting an exponential function to the surface brightness profile of the bright inner disc (corresponding to the region where highly structured spiral arms and dust lanes are visible in Fig.1), we find that the projected scalelength varies with wavelength from  $r_{\text{inner},B} = 4.2 \text{ arcsec}$  to  $r_{\text{inner},z} = 1.3 \text{ arcsec}$ . The steeper outer profile is very similar in all bands, with exponential scalelength of  $\sim 0.55 \text{ arcsec}$ . Beyond 5 arc-

<sup>1</sup> For  $H_0 = 70 \text{ km sec}^{-1} \text{ Mpc}^{-1}$ ,  $\Omega_0 = 1$ ,  $\Omega_\Lambda = 0.7$

<sup>2</sup> Available from <http://www.stsci.edu/hst/udf/release>

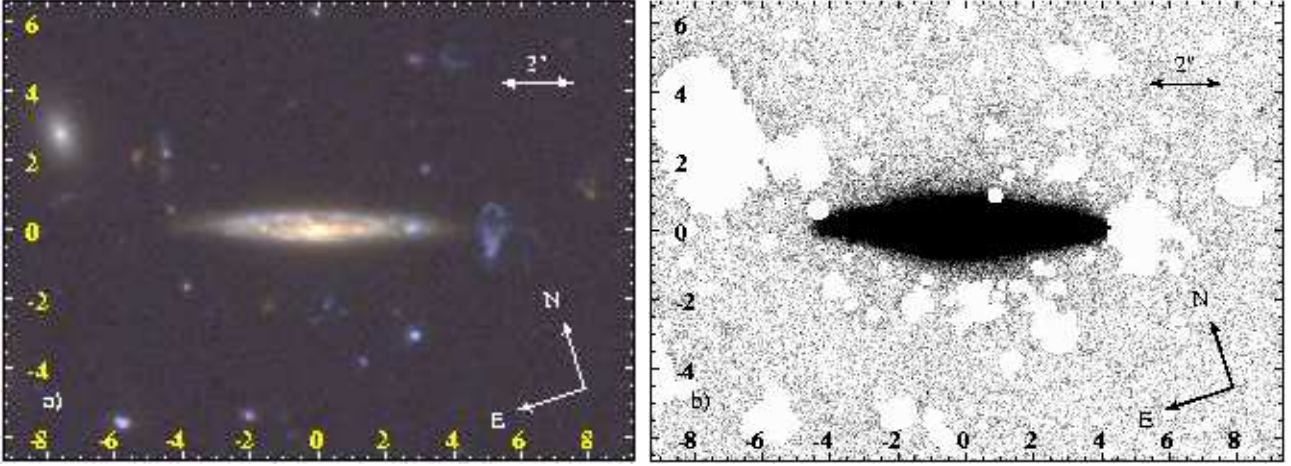


**Figure 1.** a) Full resolution colour composite RGB (( $i+z$ )- $V$ - $B$ ) image of the galaxy showing whole dynamic range. b)  $i+z$  band inverted gray-scale image, with enhanced contrast in the low surface brightness levels and masked regions superposed. Intensity scaling is a square root function in both panels. Axes show the offset in arcseconds with respect to the galaxy centre.

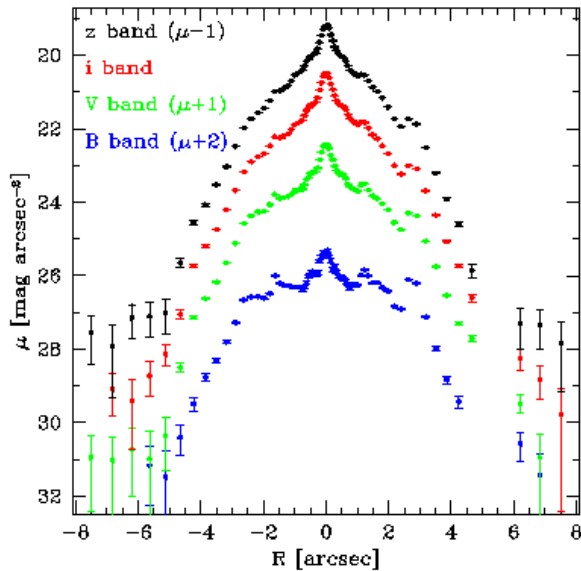


**Figure 2.** Major axis surface brightness profiles. Negative  $R$  are used for the eastern side, positive for the western. Error bars are computed as explained in the text. Only points with  $S/N > 1$  are plotted. The profiles for the different bands are coded in different colours and offset in order to avoid confusion, as indicated in the legend.

sec an excess with respect to the exponential profile is seen in the three reddest bands at the level of  $\mu \sim 29 - 30$  mag arcsec $^{-2}$ .

The minor axis profile is extracted using wedges aligned with the the  $+y$  and  $-y$ -axes and with a wider opening angle of  $45^\circ$  in order to ensure adequate  $S/N$  far from the disc plane (see Fig. 3). On the southern side of the galaxy, the inner profile is more regular and declines as a smooth exponential until approximately 0.5 arcsec. Beyond 1 arcsec, a significant power-law excess is apparent (on both sides of the plane) in all four bands (see Fig. 3). The slope of this power-law component is measured to be  $\sim 2.6$  in the

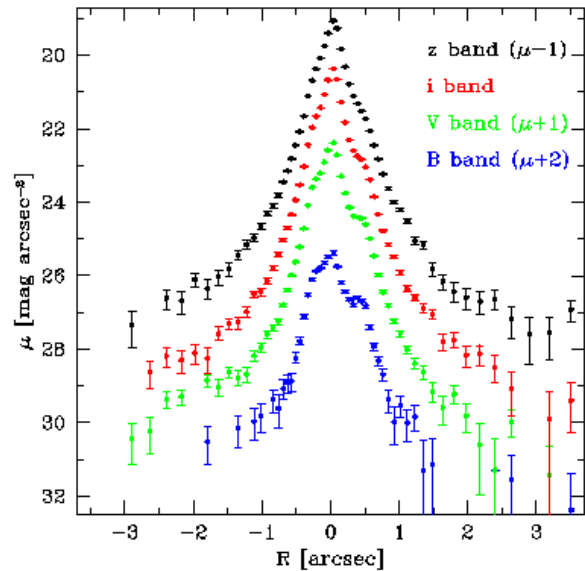


**Figure 3.** Same as Fig.2 for the minor axis. Negative  $R$  are used for the southern side, positive for the northern.

three reddest bands; we expect the effect of dust (as well as emission from an inclined disc) to be minimal at these heights ( $\gtrsim 5$  kpc) from the midplane.

We have checked that the point spread function (PSF) does not have a significant effect on our derived profiles by studying the surface brightness profile of a relatively bright, unsaturated star ( $m_V \sim 20.5$  mag) which falls within the UDF. We find that the surface brightness drops by  $\gtrsim 10(12)$  mag arcsec $^{-2}$  from the centre to 1 (2) arcsec in all bands. As a result, scattered light from the central PSF should be well below our measurement uncertainties.

In order to estimate the isophotal ellipticity of the power-law component, we measure the surface brightness as a function of radius in narrow wedges ( $13^\circ$  wide) placed at different position angles. By comparing surface bright-

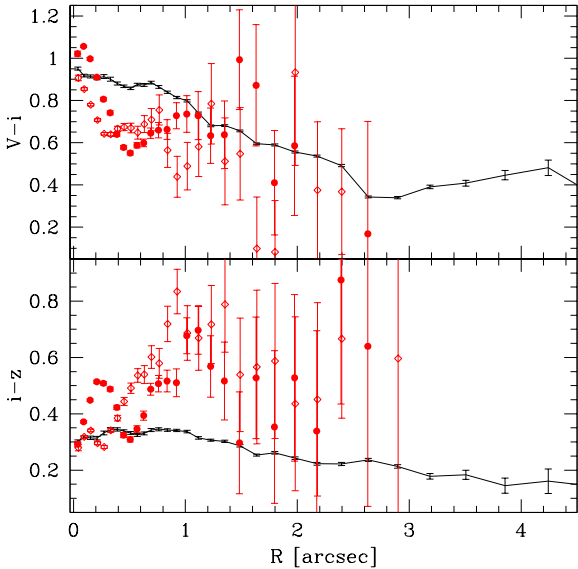


**Figure 4.** Colour profiles:  $V-i$  (top),  $i-z$  (bottom). Black solid lines represent the major axis and red points represent the minor axis (filled circles for the northern side, open diamonds for the southern). See text for details.

nesses as a function of position angle out to a radius of 5.5 arcsec, we derive an axial ratio of  $b/a \sim 0.45$  in the  $i$ -band at  $\mu_i \sim 29$ . The outermost isophotes thus appear significantly rounder than the inner (disc-dominated) isophotes. Our measurement represents a lower limit on the actual flattening however, since low-level disc emission may still contaminate the isophotes at 0 and  $180^\circ$ . Indeed, if we exclude the sectors which lie within  $25^\circ$  of the major axis, the ellipticity  $b/a$  of the faint outer component increases to 0.6.

In Fig. 4 we plot the  $V-i$  and  $i-z$  colours along the major (black solid line) and minor axes (red points) as obtained from combining the surface brightness profiles shown in Figures 2 and 3. The major axis profile represents the average of the eastern and western axes in regions where  $S/N > 2$ . Error bars are attached using the standard propagation of the errors on the surface brightness measurements. The profiles along the major axis display a clear blue gradient in  $V-i$  within  $\sim 2.5$  arcsec, where the bright disc dominates. Beyond  $\sim 3$  arcsec, where the exponential slope significantly steepens, the gradient in this colour is inverted. The  $i-z$  profile is significantly flatter, slowly varying from 0.3–0.35 in the inner 1 arcsec, to 0.15 at 4 arcsec.

For the minor axis, the north and south sides are shown separately as filled circles and open diamonds respectively. Along the minor axis we observe a clear blue gradient in  $V-i$  within  $\sim 0.5$  arcsec, while the  $i-z$  profile in this region is very irregular and likely reflects both internal structure as well as dust within the disc. The transition between the disc and power-law regions is characterised by a strong red gradient in  $i-z$ , from 0.4 at 0.5 arcsec to 0.7 at 1 arcsec (considering the average of the northern and southern profiles). In the region dominated by the power-law excess ( $R \gtrsim 1.5$  arcsec), the colour measurements are rather noisy due to the very low surface brightness, but still there is evidence for  $V-I \sim 0.6 - 0.7$  and  $i-z \sim 0.5 \pm 0.1$ .

We also estimate the total magnitude of the galaxy, of the disc alone, and of the galaxy excluding the disc in each band (see Table 1). The total magnitude is integrated in an ellipse with  $b/a = 0.6$ ,  $a = 8$  arcsec, while for the disc alone we adopt an ellipse with  $b/a = 0.2$ ,  $a = 4.8$  arcsec. The “Total-Disc” magnitude is integrated in the complementary region. Typical uncertainties are of order of 0.05 for the “Total-Disc”, essentially given by count statistics and background uncertainty. In the three reddest bands the contribution of the non-disc component ranges from 4.3 to 5.6 per cent of the total light and displays colours which are significantly redder than those of the disc, namely  $V-i = 0.73 \pm 0.10$  vs.  $0.64$  and  $i-z = 0.52 \pm 0.10$  vs.  $0.33$ . Reddening due to dust is unlikely to affect the colours at these radii and, in any case, any realistic distribution of dust would lead to bluer colours with increasing distance from the disc instead of redder ones.

## 4 DISCUSSION

Our analysis of the UDF galaxy, COMBO-17 #31611, has yielded the detection of a very low surface brightness structural component in addition to the bright disc. The main evidence for this component is: *i*) excess emission with respect to an exponential profile detected to 3 arcsec ( $\sim 14$  kpc) from the disc plane at the level of  $\mu_{V,i} \sim 29$  mag arcsec $^{-2}$ ; *ii*) the isophotal shape is centrally-concentrated and becomes rounder with increasing radius, reaching  $b/a \sim 0.6$  at the faintest measured isophote; *iii*) colours far from the plane that are distinct from the disc, i.e.  $i-z \sim 0.5$  and  $V-i \sim 0.7$  which are 0.2–0.3 and 0.1 mag redder than the disc respectively. Based on these properties, we attribute this component to the stellar halo of the galaxy, making it the most distant detection of a stellar halo yet known. We note the striking resemblance between the halo properties derived here and those of the “mean” halo detected in Z04’s SDSS stacking analysis. As discussed in Z04, these observations are also consistent with the few extant observations of individual stellar haloes.

The surface brightness profile of the halo is consistent with a power-law falling as  $I \propto R^{-2.6}$ . This slope must be considered an upper limit since if there is contaminating outer disc emission within our aperture, it will steepen the observed profiles even beyond 1 arcsec. An  $R^{1/4}$  law provides a poor fit to the data, which display excess emission at the faintest surface brightness levels compared to this profile. Less concentrated Sérsic profiles, which are more appropriate for the small bulges of late-type galaxies, provide even worse fits, thus ruling out the bulge as responsible for the measured emission. The fractional contribution of the halo to the total galaxy light is around 5 per cent, but this should be considered only approximate since we neglect disc contamination in the region where the halo light is integrated and include the inner halo as part of the disc light. Furthermore, we have no handle on internal extinction which could be significant in the inner regions of the galaxy, where the disc contribution is calculated.

In order to conduct a direct comparison between the surface brightness and colours of this distant stellar halo and those of local galaxies, corrections need to be applied for bandpass shifting and surface brightness dimming. Given

**Table 1.** Integrated photometry and colours: the total and disc fluxes are integrated in elliptical apertures, as described in the text. For the “Disc” and “Total–Disc” components, the percentage over the total flux are given as well.

	V		i		z		V – i	i – z
	mag	%	mag	%	mag	%	mag	mag
Total	21.14		20.50		20.16		0.64	0.34
Disc	21.18	95.7%	20.55	95.4%	20.23	94.4%	0.64	0.33
Total–Disc	24.54	4.3%	23.82	4.6%	23.30	5.6%	0.73	0.52

the photometric redshift of 0.322, the four observed bands, *BViz* correspond rather well to the SDSS *ugri* bands at redshift zero. Assuming a 9 Gyr,  $Z = 0.4Z_{\odot}$  single stellar population (SSP), we use the Bruzual & Charlot (2003) (hereafter BC03) models to calculate that observed surface brightnesses in *Viz* translate into rest-frame values of  $\sim 1.1$  mag arcsec $^{-2}$  brighter in *gri*. Our measurements of  $\mu_{V,i,z} \sim 29 - 30$  mag arcsec $^{-2}$  thus correspond to rest-frame equivalents of  $\mu_{g,r,i} \sim 28 - 29$  mag arcsec $^{-2}$ . This is precisely the surface brightness range in which a power-law halo component starts to dominate the minor axis profile in Z04’s SDSS stacking analysis and in which direct detections of individual haloes have been made in nearby galaxies.

We proceed to use the BC03 models to interpret the colours of the halo emission in terms of stellar populations. First, we compare the observed colours with predictions for different SSPs with ages of 2–13 Gyr and metallicities of 0.005–2.5  $Z_{\odot}$  adopting a Chabrier (2003) Initial Mass Function (IMF). We find none of these models can simultaneously reproduce the intermediate  $V - i$  and the very red  $i - z$  colours. Unless a super-solar metallicity is assumed ( $Z = 2.5Z_{\odot}$ ), the measured  $i - z \sim 0.5$  is at least 0.15 mag redder than the models and thus inconsistent at more than the 1.5  $\sigma$  level. Such an anomaly is reminiscent of the finding of a correspondingly high  $r - i \sim 0.6$  by Z04, despite the intermediate  $g - r \sim 0.65$  that could be accounted for by an old population with roughly solar metal enrichment.

Since we have been unable to produce a model that provides a good fit to the observed colours at  $z = 0.32$ , we adopt the following strategy to derive rest-frame colours that can be compared to haloes in the local universe. We adopt a fiducial reference model of an SSP of age 9 Gyr at the redshift of the galaxy, with  $Z = 0.4 Z_{\odot}$ , and a Chabrier IMF (BC03); this model minimises the absolute deviations from the observed colours. We then evolve the spectrum to  $z = 0$  and derive the rest-frame colours that would be observed through SDSS *gri* passbands. These colours can then be directly compared to the measurements of Z04 for the “mean” halo in their SDSS stack. Not unexpectedly, the evolved colours do not provide a good match to Z04’s observations but interestingly the offset between the model and observations is of the same magnitude and sense at  $z = 0$  as at  $z = 0.32$ . Specifically, while the model predicts a blue colour ( $V - i$  or SDSS  $g - r$ ) that is consistent or just slightly redder than the observations, the predicted red colour ( $i - z$  or SDSS  $r - i$ ) is too blue by  $\sim 0.2$  mag.

This kind of colour anomaly, i.e. too much flux in the spectral region around 7500Å with respect to shorter optical wavelengths, was also seen in the stellar halo of the nearby system NGC 5907 Lequeux et al. (1998). An attempt to directly resolve the population of metal-rich giant stars that

would give rise to these red colours was unsuccessful, leading to the suggestion that the stellar halo in NGC 5907 formed with a non-standard IMF that is dominated by  $M \lesssim 0.2M_{\odot}$  stars (Zepf et al. 2000). While such a truncation could account for the lack of halo giant stars, it is unclear whether it could also explain the colours observed here, i.e.  $g - r$  typical of G-K stars yet  $r - i$  typical of M stars. Another possibility is that the red colour is contaminated by ionised gas emission. Deep  $H\alpha$  imagery of nearby galaxies often reveals faint extraplanar emission (Ferguson, Wyse, & Gallagher 1996; Miller & Veilleux 2003), however little is known about the extent of these ionised “haloes” at very faint flux levels. Further investigation is clearly required in order to understand the origin of the peculiar halo colours, which have now been measured in three independent studies.

As a final remark, we note that the surface brightness profile of the disc can be fitted by an exponential function that changes scalelength abruptly at 3 arcsec  $\simeq$  14 kpc (corresponding to  $\sim 2.4$  inner scalelengths). This behaviour is consistent with deep imaging studies of both edge-on and face-on discs in the local universe (Kregel et al. 2002; Pohlen et al. 2002) and likely reflects a truncation of the bright inner disc. That this radius also represents the point where the major axis colour gradient reverses and starts to redden is intriguing and suggests that the stellar populations at the far extremity of the disc are of significant age.

We thank the referee, Michael Pohlen, for useful comments. The research of AMNF has been supported by a Marie Curie Fellowship of the European Community under contract number HPMF-CT-2002-01758.

## REFERENCES

- Abadi, M. G., Navarro, J. F., Steinmetz, M., & Eke, V. R. 2003, *ApJ*, 597, 21  
Abe F., et al., 1999, *AJ*, 118, 261  
Beckwith S., Somerville R., Stiavelli M., 2003, *STScI Newsletter*, Vol 20, Issue 04, p1  
Bertin E., Arnouts S., 1996, *A&AS*, 117, 393  
Bruzual G., Charlot S., 2003, *MNRAS*, 344, 1000 (BC03)  
Bullock, J. S. & Johnston, K. V. 2004, in proceedings of “Satellites and Tidal Streams”, eds. F. Prada, D. Martinez-Delgado & T. Mahoney, astro-ph/0401625  
Chabrier G., 2003, *PASP*, 115, 763  
Dalcanton J. J., Bernstein R. A., 2002, *AJ*, 124, 1328  
Ferguson, A. M. N., Wyse, R. F. G., & Gallagher, J. S. 1996, *AJ*, 112, 2567  
Ferguson A. M. N., Irwin M. J., Ibata R. A., Lewis G. F., Tanvir N. R., 2002, *AJ*, 124, 1452

- Fry A. M., Morrison H. L., Harding P., Boroson T. A., 1999, *AJ*, 118, 1209
- Kregel M., van der Kruit P. C., de Grijs R., 2002, *MNRAS*, 334, 646
- Lequeux J., Combes F., Dantel-Fort M., Cuillandre J.-C., Fort B., Mellier Y., 1998, *A&A*, 334, L9
- Miller, S. T. & Veilleux, S. 2003, *ApJS*, 148, 383
- Morrison H. L., Miller E. D., Harding P., Stinebring D. R., Boroson T. A., 1997, *AJ*, 113, 2061
- Pohlen M., Dettmar R.-J., Lüticke R., Aronica G., 2002, *A&A*, 392, 807
- Sackett P. D., Morrison H. L., Harding P., Boroson T. A., 1994, *Nature*, 370, 441
- Schlegel D. J., Finkbeiner D. P., Davis M., 1998, *ApJ*, 500, 525
- Wolf, C., et al. 2004, *A&A* submitted, astro-ph/0403666
- Zepf S. E., Liu M. C., Marleau F. R., Sackett P. D., Graham J. R., 2000, *AJ*, 119, 1701
- Zheng Z., et al., 1999, *AJ*, 117, 2757
- Zibetti S., White S. D. M., Brinkmann J., 2004, *MNRAS*, 347, 556 (Z04)